2022

Contact Simulation for Evaluating Patient Specific Surgical Guide Stability

Vincent Nierste
University of Denver

Contact Simulation for Evaluating Patient Specific Surgical Guide Stability

Abstract

This study proposes a novel computational method to quantify guide stability for Patient Specific Instrumentation (PSI) guides. A finite element contact model was used to analyze the final position of PSI guides on a femur across a range of loading parameters representing forces applied by a surgeon during operative use. Separate segmentation methods were used for the guide and bone geometry to represent differences between segmentation and actual patient geometry. The region of loading parameters over which the guide exhibited a consistent final position was measured and reported as Guide Stability Score. The model was verified using cadaver specimens for which 3D printed PSI guides were applied to the knee using similar variations in guide loading. A strong correlation was found between the Guide Stability Score and the variance seen in the lab ($R2 = 0.84$), suggesting the model provides a useful tool for the evaluation of PSI guide stability.

Document Type

Thesis

Degree Name

M.S.

Department

Mechanical Engineering

First Advisor

Chadd Clary

Second Advisor

Paul Rullkoeter

Third Advisor

Mei Yin

Keywords

Contact simulation, Patient specific guide, Total knee arthoplasty

Subject Categories

Biomechanical Engineering | Biomedical Devices and Instrumentation | Mechanical Engineering

Contact Simulation for Evaluating Patient Specific Surgical Guide Stability

_____

A Thesis

Presented to

the Faculty of the Daniel Felix Ritchie School of Engineering and Computer Science

University of Denver

_____

In Partial Fulfillment

of the Requirements for the Degree

Master of Science

_____

by

Vincent Nierste

November 2022

Advisor: Dr. Chadd Clary

Author: Vincent Nierste
Title: Contact Simulation for Evaluating Patient Specific Surgical Guide Stability
Advisor: Dr. Chadd Clary
Degree Date: November 2022

Abstract

This study proposes a novel computational method to quantify guide stability for Patient Specific Instrumentation (PSI) guides. A finite element contact model was used to analyze the final position of PSI guides on a femur across a range of loading parameters representing forces applied by a surgeon during operative use. Separate segmentation methods were used for the guide and bone geometry to represent differences between segmentation and actual patient geometry. The region of loading parameters over which the guide exhibited a consistent final position was measured and reported as Guide Stability Score. The model was verified using cadaver specimens for which 3D printed PSI guides were applied to the knee using similar variations in guide loading. A strong correlation was found between the Guide Stability Score and the variance seen in the lab ($R^2 = 0.84$), suggesting the model provides a useful tool for the evaluation of PSI guide stability.

Acknowledgements

This thesis and research would not have been possible without the support of DePuy Synthes and the TruMatch group. Many thanks to those who assisted in the cadaver lab planning and execution. Thank you also to my advisor, Dr. Chadd Clary, who provided countless sessions assisting the development of the computational model developed herein.

Table of Contents

List of Figures

Chapter Two

List of Tables

Chapter One: Literature Review

Patient specific instruments (PSI) are custom designed tools used by surgeons to execute a total knee replacement procedure. These guides are created using the geometry of the patient's bone so that when pressed on to the bone during surgery, they find a singular home, allowing for precise positioning of pins and cutting tools. PSI guides reduce the number of manual instrument trays needed intraoperatively, providing efficiency for the hospital, and can also help to reduce operative time for the patient (Mattei L, 2016).

The typical workflow for a surgeon to use PSI guides begins pre-operatively. The surgeon will send a patient for either Computed Tomography (CT) or Magnetic Resonance Imaging (MRI) to obtain a full scan of the patient's knee and leg geometry. This information is then sent to the manufacturer for segmentation, the process by which 3D geometry is created from the imaging. The segmented knee joint is then used to create a surgical plan that is customized for the patient, using bony landmarks to define resection levels and alignments for the knee replacement surgery. Once the surgeon approves this pre-operative plan, the surgical guides are designed, manufactured, and shipped to the surgeon for operative use.

Guide positioning can be improved with a robust surgical technique, training, and experience, but even with perfect execution, a surgeon can experience fit issues between the guides and bones during surgery. These fit issues include but are not limited to the presence of soft tissue interference, cartilage segmentation inaccuracy, and the presence of bony growths called osteophytes. Studying fit issues experienced by a surgeon is traditionally a resource intensive exercise that involves both cadavers and surgeons, creating a situation that is prime for computational analysis.

Computational tools can be used to analyze guide geometry optimization, touch point optimization, and guide positioning optimization among other factors. Even if a computational model doesn't perfectly replicate use of PSI in an operation, it can help identify the factors that most strongly correlate with surgical success. For guide geometry optimization, a computational tool could help cull a wide variety of prototype guide designs down to just a few of the most robust designs for full evaluation with surgeons and cadavers. For guide positioning technique, the same tool could help to identify the most common errors or pitfalls for surgeons to avoid even if an absolute best technique cannot be identified.

Quantification of the accuracy of PSI guides is a challenging problem and one that has been explored in the literature by both researchers and surgeons. Several methods have been used to study the operative use errors in PSI guides, including intraoperative radiographs, postoperative CT, and novel methods that utilize high visibility points on the patient anatomy for intraoperative verification (Mueller S, 2016) (Kunz M, 2010). These

methods are still resource intensive and rarely allow for direct comparison of guide designs, making a computational model even more desirable.

Using computational tools to model PSI guide fit has been explored by a small cohort of researchers across a variety of applications in trauma, hip, glenoid, and knee applications. The primary method of analysis found in the literature revolves around the wrench space method. This concept uses the application of forces and moment arms to determine the threshold at which the guide can be dislodged from the desired position on the bone.

Van den Broeck et al used wrench space analysis to score PSI guides based on their ability to resist applied forces or moments to the guide. Two stability metrics, one for translation and one for rotation, were recorded for each guide. Based on a combination of these two metrics, various guide designs were evaluated and scored to determine their relative stability. Van den Broeck also validated this model experimentally by applying precise loads and moments to the 3D-printed guide designs and was able to show positive correlation between the resistance of guides to either translation or rotation and the corresponding scoring metrics.

Mattheijer et al built upon the approach used by Van den Broeck et al by exploring the robustness of femur guide design specifically as it related to contact area with the bone. Starting with full contact between guide and bone, the angular range of applied forces over which the guide remained in the starting position served as a scoring mechanism for each analysis. As contact points were optimized and removed between the guide and bone, a reduced range of applied loading angles resulted in a stable guide

position. This study showed that twelve points of contact maintained high robustness of fit while reducing the complexity of guide design such that the full bone surface didn't need to be recreated on the surgical guide.

Giles et al used wrench space analysis to experimentally evaluate a commercially available shoulder PSI product. This study expanded on previous work by using springs to apply a compressive load between the guide and bony geometry before applying transverse loads and moments to the guide. A guide was considered out of position when displacement of 2 mm or 5° was observed. The resistances of the guides to each of the two transverse loads and three applied torque vectors were compared to show the relative stability of the shoulder PSI in each axis, revealing that the product was relatively unstable to moments applied about the lateral axis.

All three methods seek to quantify the stability of the guide in different ways, and each has merits and flaws. One of the flaws is that these approaches all assumed that the fit between guide and patient geometry is perfect. In reality, this is a simplifying assumption and limits the application. As discussed previously, the processes of segmentation, planning, and manufacturing can each generate errors that eliminate the possibility of a perfect fit between guide and bone. These imperfections cause issues with the real-world application of these analyses for guide performance. Without a perfect geometric fit, the ability of a guide to resist rotations and translations is significantly diminished, increasing the risk of misalignment in the guides. This could result in rotations or translations from the intended guide position that negatively affect the patient outcome. Deviations from the plan greater than 3 degrees can result in upsizing or

downsizing components, poor joint mechanics, or force an early revision surgery (Kim, 2014).

Based on the gaps and opportunities identified by this literature review, the objective of this thesis is to create a novel tool for evaluating guide designs. There is space in the research to quantify the guide fit and robustness given imperfect fit between guide and bone as this better simulates an intra-operative use case. The imperfect fit will be simulated in this analysis by utilizing 3D reconstructions of both CT and x-ray (XR) imaging of a patient. Without a perfectly aligned set of bone and guide surfaces, it is no longer obvious where the guide comes to rest on the bony surface. This mirrors clinical feedback from surgeons, indicating that sometimes PSI knee guides can have multiple positions, or “homes”, that feel correct when positioning a guide onto a patient.

A contact simulation using finite element analysis (FEA) combined with simulated applied forces by the surgeon will be used to identify the final position of a guide given imperfect fit between guide and bone. For this type of analysis, there are three main variables: Bone-guide contact area (guide design), bone imperfections representing segmentation errors, and application of force representing guide positioning technique.

For guide design, a single prototype concept will be developed for evaluation of this tool. This guide will use utilize an existing production process to identify cutting planes and alignment, but will evaluate a prototype bone contact pattern across a small sample of cadaver geometries.

For bone imperfections, an analysis of segmentation errors will be developed by comparing CT scan segmentations to XR segmentations. These two imaging technologies

have different strengths and weaknesses. Utilizing an XR model to create guides while fitting them to a CT model will create highly similar, yet not identical surfaces to study the robustness of guide design and placement.

Guide positioning technique will be represented in the FEA model by the application of one or more forces representing a surgeon's fingers or hand. An analysis of guide positioning techniques across PSI guides from different manufacturers will reveal some of the most common techniques which could then be represented in the FE analysis.

The scoring metric for this analysis will need to be different than those defined in wrench space analysis. A good scoring metric would reward guides that had the highest robustness to deviations in the three metrics defined above. This guide design would then in theory have the highest intraoperative success rate for the most patients.

Lastly, this thesis seeks to validate the model with an experimental component consisting of a cadaver lab study. The cadaver lab study will evaluate the same guide design as the computational model, relying on the differences between the true bone geometry, CT-based guides, and XR-based guides and differences in guide positioning technique to evaluate the robustness of the guide design and correlate those results with the scoring metric from the model.

Chapter Two: Evaluation of Robustness in Guide Positioning

Introduction

Patient specific instrumentation (PSI) are custom designed instruments used by surgeons to execute a total knee replacement procedure. These guides are created using the geometry of the patient's bone so that when pressed against the bone during surgery, the guide articulates into a predetermined alignment, allowing for precise positioning of pins and cutting tools. PSI guides reduce the number of manual instrument trays needed intraoperatively, providing efficiency for the hospital, and can also help to reduce operative time for the patient (Mattei L, 2016).

The typical workflow for a surgeon to use PSI guides begins pre-operatively. The surgeon sends a patient for imaging to obtain a full scan of the patient's knee and leg geometry. This information is then segmented by the manufacturer, the process by which 3D geometry is created from the imaging. The segmented knee joint is then used to create a surgical plan that is customized to each patient, setting implant resection levels and rotations. Once the surgeon approves this pre-operative plan, surgical guides which conform to the unique patient geometry are designed, manufactured, and shipped to the surgeon for operative use. These guides serve to align pins and resection planes according to the preoperative plan.

One of the issues that can occur with PSI is misalignment of the guide during surgery. Inaccuracies in the segmentation process or progression of osteoarthritis in the patient after the scan can lead to discepancies between the geometry used to create the PSI guide and the true patient anatomy. Furthermore, variations in guide positioning technique during the application of the guide to the bone (i.e. applying different loading via the guides touch points) can lead to errors guide placement. Anecdotally, these factors can also make guides feel stable in more than one position, or "home". If the guide is not accurately fit onto the femur or tibia, it can affect the final implant position, resulting in misalignment, resection errors, or revision following surgery (Kim, 2014).

Quantification of the accuracy and stability of PSI guides is a challenging problem that has been investigated in the literature by both researchers and surgeons. Several methods have been used to study intraoperative use errors in PSI guides, including postoperative computed tomography (CT), intraoperative radiographs (Mueller S, 2016), and novel methods that utilize high visibility points on the patient anatomy for intraoperative verification (Kunz M, 2010). These methods are resource intensive, requiring guide use in actual patients or cadaveric specimen, and rarely allow for direct comparison of guide positioning techniques or guide designs, making a computational model highly desirable.

Van den Broeck et al (2015) and Mattheijer et al (2015) have described computational models centered around robotic grasping analyses which successfully predicted guide resistance to applied forces and moments for various PSI guide

applications, but none of these studies incorporated non-identical geometry between the guide and bone.

This study proposes a novel computational method to quantify guide stability for predicting the robustness of PSI femur guides to variations in guide positioning techniques. A finite element (FE) model was used to predict the final position of PSI guides given a range of guide loading applied by the surgeon. The model was verified using cadaver specimens for which 3D printed PSI guides were applied to the knee by multiple observers using variations in guide loading.

Materials and Methods

This study included both experimental and computational components. In both parts of the study, computed tomography (CT) data and x-ray (XR) data from the same specimens were used to create two sets of bone geometry for four specimens. The bone geometries imaged consisted of the distal femur, proximal tibia, and proximal fibula.

For the CT scans, slices were taken at 1 mm thickness through the knee and at 5 mm thickness elsewhere in the long bone scan. For the XR scans, three scans were acquired: an anterior-posterior radiograph of the knee, a lateral radiograph of the knee, and a synthetic long-leg AP radiograph that was generated from the CT scan. Each set of imaging data were segmented into three-dimensional bony geometry.

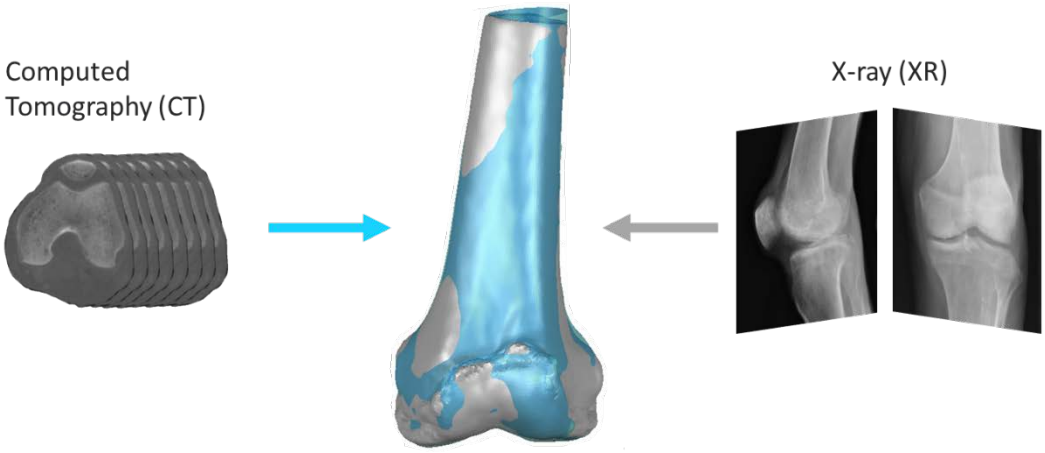

Figure 1: Two different segmentation methods were used to generate highly similar 3D models of a single specimen's knee.

The segmented bones were processed through the TruMatch® Patient Specific Guides (Depuy Synthes, Inc) model creation process to generate both femur and tibia preoperative plans and PSI guides from both the CT-based and XR-based geometry for each specimen. The TruMatch guides served as the baseline design for the PSI guides, defining the planned resection levels and implant alignments in this study. The baseline guides were then modified using the NX 12 software package and represented a prototype, non-production guide design (Figure 2). The processes used to create the CT- and XR-based PSI guides were identical except for the segmentation method used. In total, this resulted in 8 femur guides. After the guides were digitally created, the femur guides were exported to .stl files and 3D printed for use in a cadaver lab.

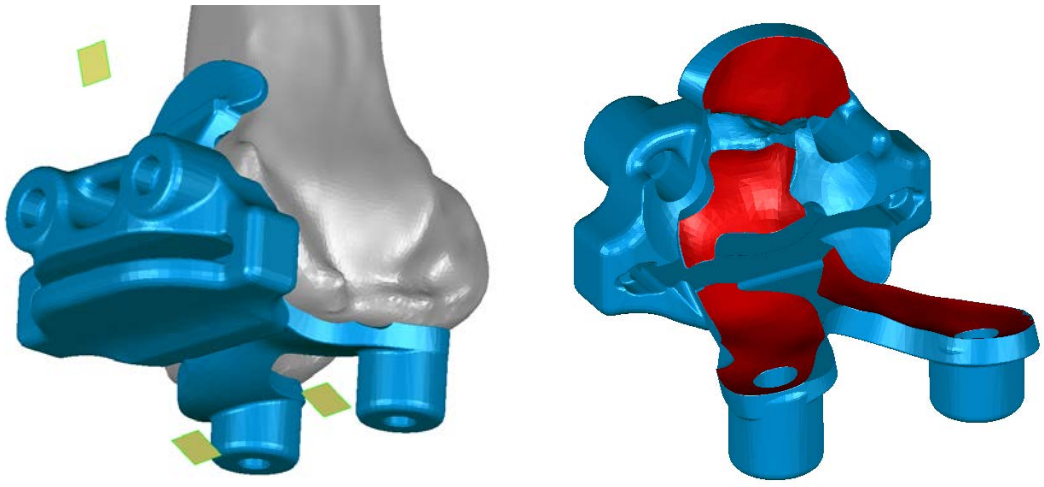

Figure 2: Depiction of prototype guide design. On left, squares show the anterior and distal touch points (yellow) used to apply the guide to the bone during the analysis and lab. On right, red highlighted regions of the guide show areas designed to contact bony surfaces.

Experimental Model - Cadaver Lab

A cadaver lab was set up for evaluation of the 3D printed PSI guides. During setup for each cadaver, the Brainlab Knee3 Computer-Assisted Surgery (CAS) system was used to develop a coordinate system and take measurements of guide accuracy repeatedly without performing resections on the bones under analysis. Keeping consistent bony registration between all trials allowed for direct comparison of guide accuracy by changing operator and method on the same bone before moving on to the next specimen.

Guide Positioning Technique Evaluation

The primary experiment performed during the cadaver lab utilized the XR-based guides to test variations in guide positioning techniques and their effect on guide placement and accuracy. Each operator placed the guide according to five different methods (Figure 3), comprising the center and four corners of a loading design space which varied force distribution and angle. The “anterior” methods emphasized loading on

the anterior touch point, while the “distal” techniques emphasized loading on the distal touch points of the guide. “Extension” methods focused on pushing the guide into extension, toward the posterior direction while “flexion” methods focused on pushing the guide into flexion, toward the superior direction. The “neutral” method provided balanced pressure directed in between the superior and posterior directions. In addition, CT-based guides were evaluated in the “neutral” guide placement method.

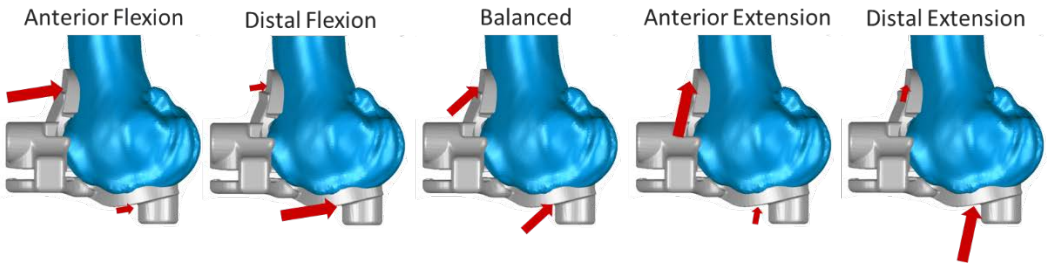

Figure 3: Illustration of the applied force in each of the 5 methods performed during the cadaver lab. Methods labeled “anterior” placed emphasized force applied to the anterior surfaces, while “distal” methods emphasized force applied to the distal surfaces. Flexion and extension represent the direction of force applied to the guide.

The neutral technique was repeated three times for each operator for both the CT and XR-based guide. This was followed by a single trial of each of the five guide placement techniques using the XR-based guie, resulting in each operator placing the XR-based guides eight times each and the CT-based guides three times each. Once the operator felt that the guide was placed on the bone according to the prescribed method, the computer-assisted surgical system was used to measure the distal resection plane as set by the guide. Distal plane flexion angle and distal plane varus/valgus angle values were recorded from the CAS system for each trial (Figure 4).

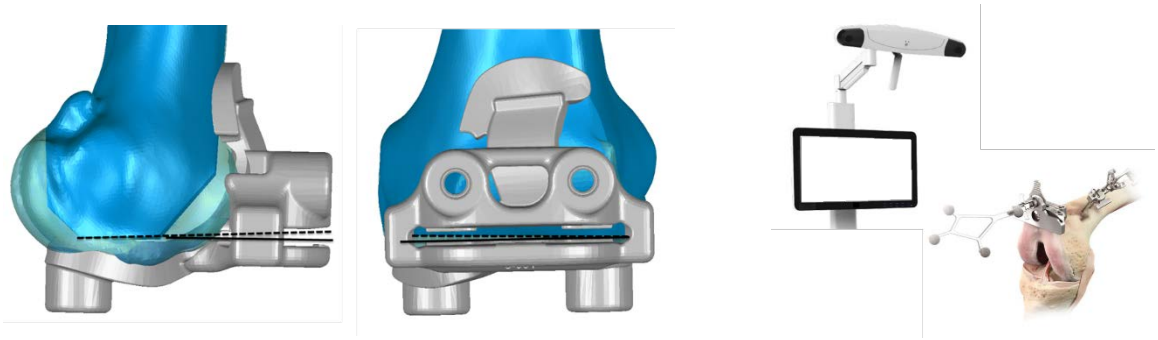

Figure 4: Flexion-extension error (left) and varus-valgus error (center) were captured with a CAS system (right) during the cadaver lab for each iteration of guide placement.

Computational Model Formulation

The computational model focused on evaluating a range of guide loading conditions that could be used to apply the femur guide to the corresponding bone. Each model consisted of the femur bone, derived from the CT scan, and either the XR-based or CT-based femur PSI guide. The femur bone and guide were meshed with 0.75-mm triangular elements. Contact between the bone and guide was defined via a pressure-overclosure relationship with a stiffness of 141 N/mm and used a coefficient of friction of 0.1 to improve run time (Halloran JP, 2005) compared to a deformable model of the bone and cartilage. Sensitivity analyses were performed to determine the effect of the pressure-overclosure model parameters, mesh density, mass scaling, and friction on the resulting guide alignment.

Geometric Setup

An iterative closest point (ICP) alignment was performed using the VTK 8.1.2 library in Python 3.7 to register the XR-derived bone to the CT-derived bone and used to establish the XR-guide's initial alignment. The guide was translated in the anterior and distal direction until no overclosure was detected. The result of this process was that the

guide's initial position was rotationally aligned to the planned distal and posterior resection planes.

After positioning each guide, three 8mm x 8mm squares located at the anterior, distal medial, and distal lateral touch points were created and rigidly connected to the guide geometry (Figure 2). These touch points ensured consistent loading between each guide and were excluded from the contact definition.

Once the final geometry had been created, one more sensitivity analysis was performed to determine the effect of initial guide position on the result of the contact model by creating initial displacement before applying loads to the guide. Initial displacement was applied to the guide in permutations of (±1.0mm X, ±1.0mm Y, ±1.0mm Z) before consistent loading parameters were applied to determine if the equilibrium position of the guide was deterministic or varied based on starting position.

Boundary Conditions for Contact Simulation

The femur bone was fixed in place using a reference node at the end of the segmented long bone shaft. Each guide was left free of translational and rotational boundary conditions and had loading applied to it that simulated the use of the guide by a surgeon in the operating room. A pressure load resulting in 77 N was divided between the three touch points shown in Figure 2 across two distinct steps. The first step divided the load evenly across each touch point and served to establish a baseline equilibrium position with the guide in a stable contact position with the bone, determined as having kinetic energy less than 1e-3 mJ.

To recreate a range of guide positioning techniques, loads applied to the guide were parameterized based on the angle of force application and the distribution of force between the anterior and distal touch points (Figure 5). The main analysis method focused on flexion/extension response of the guide and varied the angle parameter between 0 degrees, force being directed posterior, and 90 degrees, force being directed superior. The distribution parameter for this analysis specified the percentage (0% to 100%) of the total load that was applied to the anterior touch point of the guide, with the remainder split evenly between the distal touch points of the guide. Figure 3 displays five examples of loading configurations that can be created using these parameters. A second analysis was performed which focused on varus/valgus response of the guide. This analysis maintained 40% anterior loading and 30 deg angle of force but varied the distal force distribution between the medial and lateral condyle touch points. A separate coronal angle parameter was defined for the distal loads and varied for this analysis from 45 degrees (lateral and superior) to 135 degrees (medial and superior).

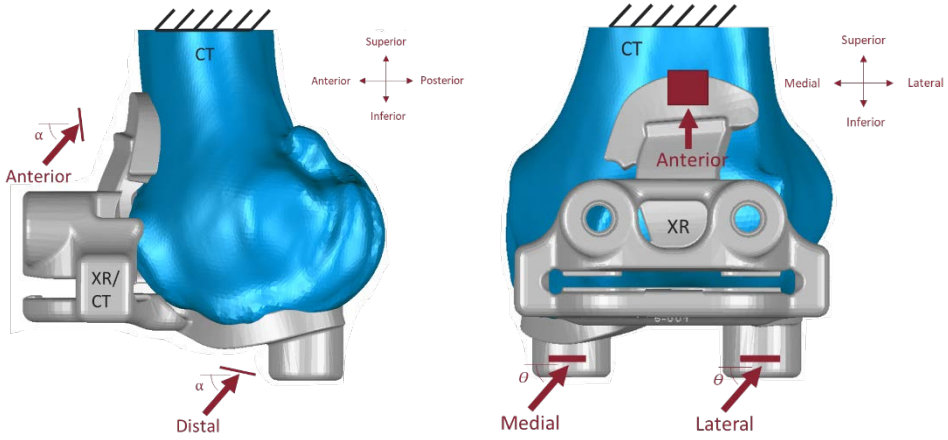

Figure 5: Diagrams of the loading conditions and parameters in the flexion-extension (left) and varus-valgus (right) analyses.

The input parameters defining the guide loading were selected via Optimal Latin Hypercube sampling across the entirety of both the flexion/extension (n=120) and varus/valgus (n=120) design spaces. In addition, the five specific loading conditions from the cadaver lab in the flexion/extension design space were evaluated.

To confirm that the model was working as expected and to establish a maximum realistic value for guide stability, the CT-based guide was paired with the CT segmented bone for evaluation. The expectation was that the perfect geometric match between the guide and bone would result in higher stability.

Data Analysis

The primary response for this analysis was the Flexion/Extension position of the guide at the end of the FEA contact model execution. Error in the model was quantified as the angular deviation in the flexion/extension axis or varus/valgus axis between the initial position of guide (translated only, no rotation) and the final position of the guide. Once this error was extracted across the entire design space, an interpolation was performed using Matlab R2013a to create a surface representing the entire design space for each guide. Regions where the error remained stable despite changes in angle and distribution represented regions of stability in the guide, commonly referred to as "homes" by the users of the guides. The size of these plateaus could be quantified by taking the gradient of the interpolated surface and isolating only the regions of the surface where the gradient was less than 0.1 deg/1 deg alpha or 0.1 deg/1% dist. The area of the design space identified by the gradient threshold created a quantifiable metric for guide stability, referred to going forward as Guide Stability Score (Figure 6).

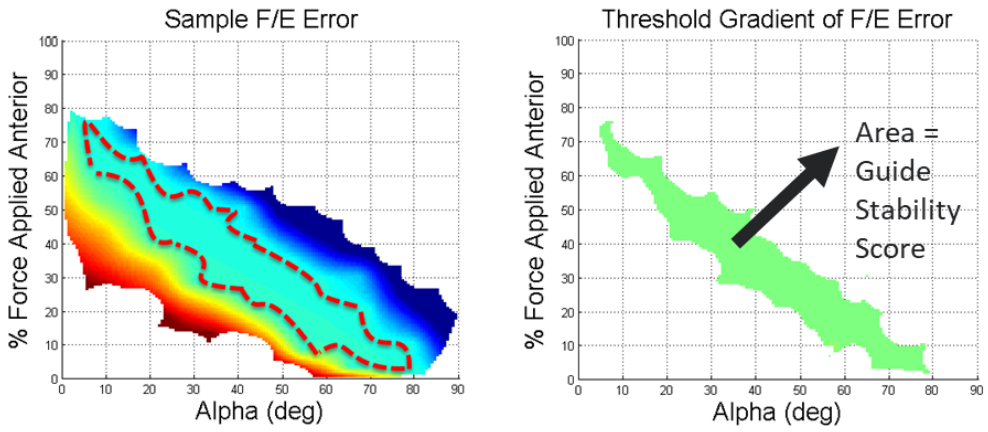

Figure 6: Sample data showing all parameter sets that resulted in contact between the guide and bone (at left) for one cadaver and the extracted sub-region (at right) identified by the gradient analysis described above as having a stable guide response.

After completing both the cadaver lab and all runs of the computational model, a comparison of the two analyses was needed. For the flexion/extension errors captured in the cadaver lab, data was separated by cadaver. For each cadaver, standard deviation and mean were calculated across all users and techniques to capture the both the accuracy and consistency of guide placement across the range of techniques used. The standard deviation from the cadaver lab was then plotted against the guide stability scores and a linear regression was performed.

Results

For the cadaver lab portion of this analysis, the mean flexion-extension error between the target and achieved guide alignments for each technique ranged from 0.2° to 7.1° and the standard deviations of the errors ranged from 2.4° to 3.4° (Table 1). All guides were biased toward flexion of the femur component with the Anterior Extension method having the lowest measured error in the flexion/extension axis when looking across all specimens. The varus-valgus error was much more consistent across all specimens and

techniques, ranging from a mean error of -1.33° to -0.71° with standard deviation of the error from 1.31° to 2.02°.

Table 1: Cadaver lab flexion/extension error. Means shown for each specimen and technique followed by the mean error and standard deviation (μ ± σ) across all samples for each technique for both XR-based and CT-based guides.

	Anterior Extension	***Anterior Flexion***	***Distal Extension***	***Distal Flexion***	***Neutral***	***Neutral – CT Guide***
Cadaver 1	2.50°	5.67°	4.00°	5.50°	4.25°	1.13°
Cadaver 2	0.50°	6.83°	4.50°	9.17°	6.67°	1.12°
Cadaver 3	-0.33°	6.17°	-0.33°	10.50°	5.17°	0.44°
Cadaver 4	-2.00°	0.83°	-1.00°	3.17°	1.83°	0.73°
All	0.17° ± 2.42°	4.88° ± 3.43°	1.79° ± 2.71°	7.08° ± 3.43°	4.48° ± 2.56°	0.85° ± 0.42°

Table 2: Cadaver lab varus/valgus error. Means shown for each cadaver and technique followed by the mean error and standard deviation (μ ± σ) across all samples for each technique.

	Anterior Extension	***Anterior Flexion***	***Distal Extension***	***Distal Flexion***	***Neutral***
Cadaver 1	0.00°	0.17°	0.00°	-0.17°	-1.71°
Cadaver 2	-2.83°	-2.83°	-3.00°	-2.50°	-2.33°
Cadaver 3	1.67°	1.33°	2.00°	1.83°	0.79°
Cadaver 4	-2.00°	-1.83°	-2.00°	-2.00°	-2.08°
All	-0.79° ± 1.84°	-0.79° ± 1.75°	-0.75° ± 2.02°	-0.71° ± 1.84°	-1.33° ± 1.31°

Figure 7 below shows the distribution of flexion/extension error across all runs, separated by cadaver specimen ID, highlighting the difference in mean and variance seen between cadavers. The data is separated into XR-based guides and CT-based guides.

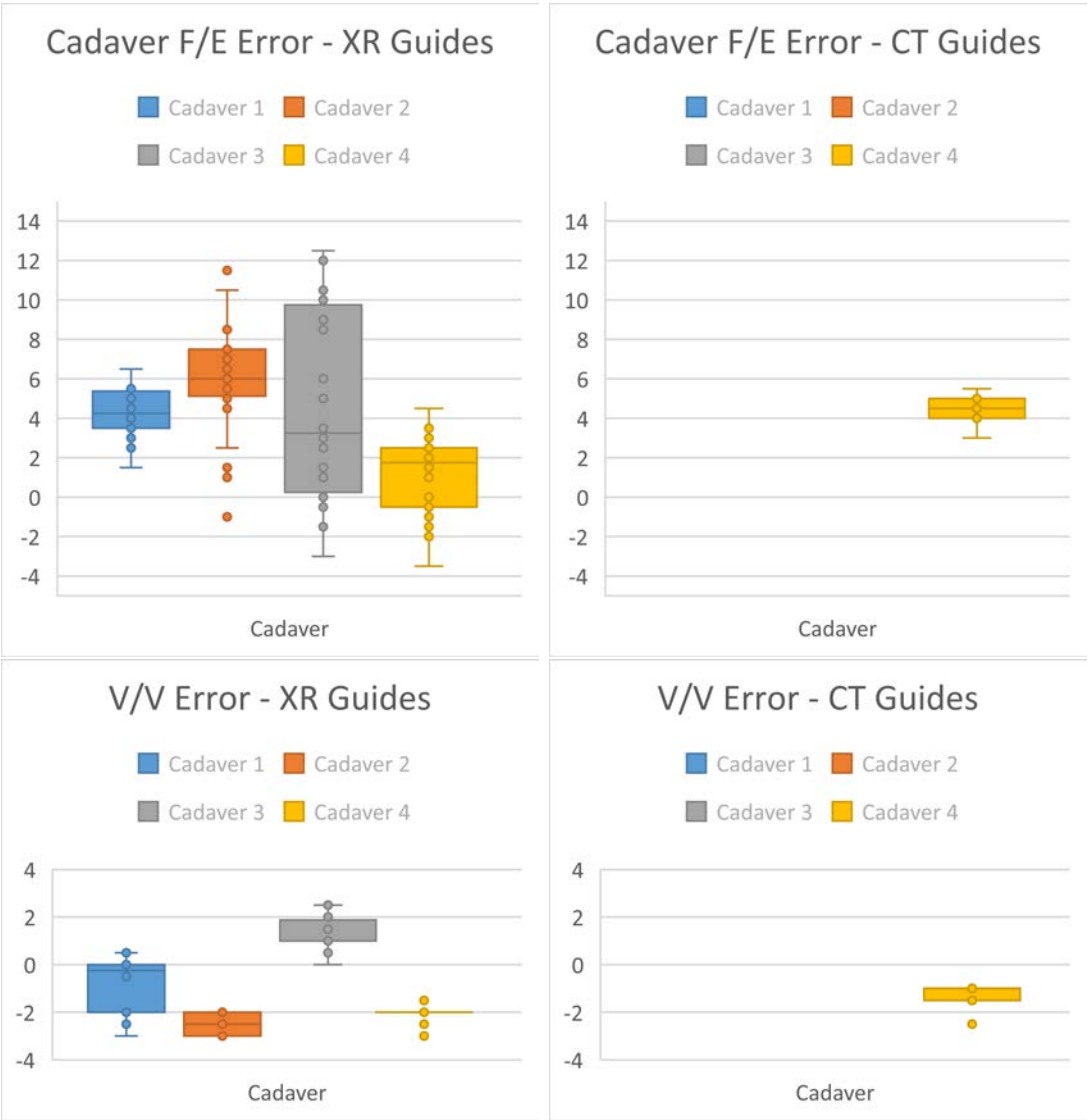

Figure 7: Flexion/extension and varus/valgus error for all users and techniques, separated by cadaver ID. For the XR-based guides, Cadavers 1 and 4 had particularly low F/E variance, while Cadaver 3 had particularly high F/E variance. For the CT-based guides, every cadaver had low F/E variance. All guides and specimens showed low variance in V/V error.

For the computational model, the Optimal Latin-Hypercube sampling of the design space revealed that only a subset of the loading evaluated in the design space resulted in a stable equilibrium position. Toward the limits of the loading parameters, the contact between guide and bone was not maintained, disengaging from the femur during the

simulation. Two representative contact area maps for a stable equilibrium position are shown below, showing the difference between XR-based and CT-based guide designs on the same femur bone. XR-based guides averaged 59.5 mm^2 contact area at equilibrium compared to 134.8 mm^2 for the CT-based guides. When comparing the stability scores of the two guide designs, the model predicts a higher stability for the CT-based guide, with a mean guide stability score of 63.1 compared to the XR-based guide, with a mean stability score of 29.9. The guide contact areas and stability scores for all XR-based and CT-based guide designs are summarized in Table 3.

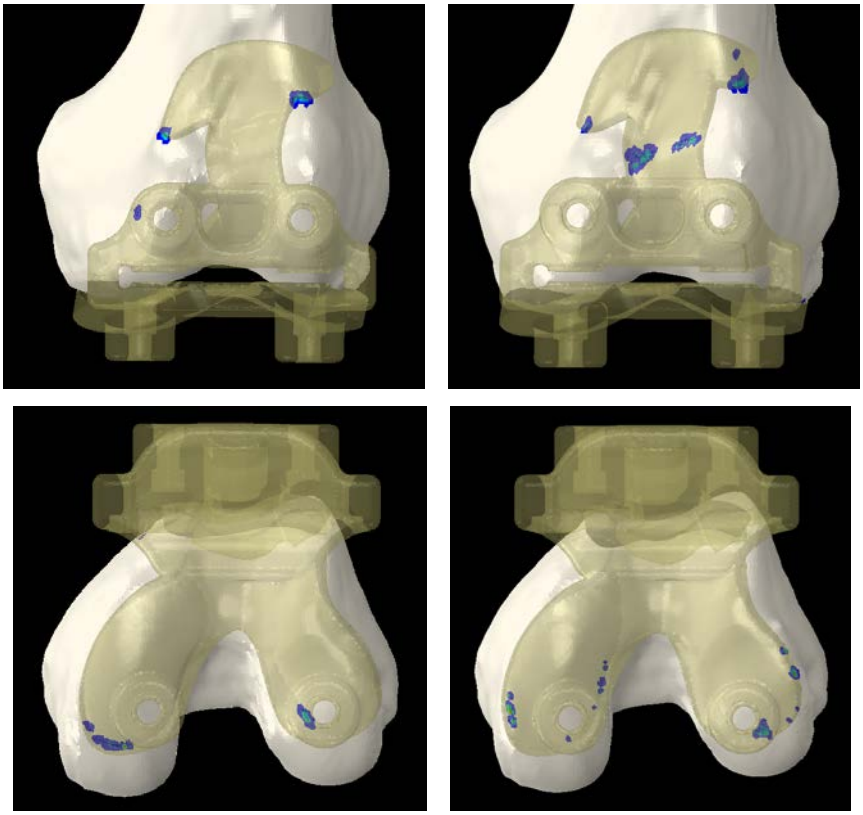

Figure 8: Representative contact pressure map for a guide and bone in equilibrium. This sample depicts Cadaver 4 in the neutral guide loading configuration with the XR-based guide on left and the CT-based guide on right.

Table 3: Guide stability scores for each of the analyses performed. Also listed are the contact areas for each of the XR-based and CT-based guides.

	XR Guide Stability Score - F/E	***XR Guide Stability Score - V/V***	***CT Guide Stability Score - F/E***	***XR Guide Contact Area***	***CT Guide Contact Area***
Cadaver 1	41.0	47.4	69.8	56.1	108.1
Cadaver 2	21.5	55.3	54.4	65.5	164
Cadaver 3	12.7	63.9	70.6	47.6	132.7
Cadaver 4	44.5	76.2	57.5	68.6	134.2
All	29.9	60.7	63.1	59.5	134.8

Differences in the geometry of the femur between XR and CT-based segmentations were calculated, showing regions of oversegmentation in red and undersegmentation in blue in Figure 9 for each femur specimen.

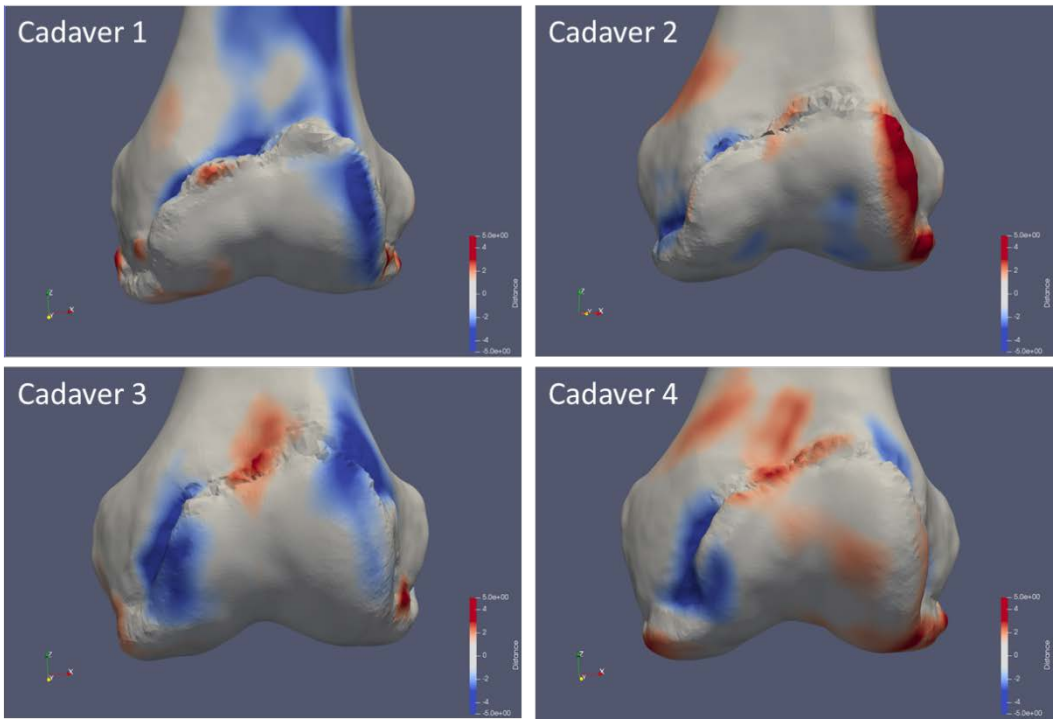

Figure 9: Differences in XR and CT segmentations. Oversegmentation greater than 3 mm is shown in dark red and undersegmentation greater than 3 mm is shown in dark blue, with a gradient in between. Segmentation errors less than 1 mm are shown in white.

Results of the F/E computational model analysis revealed large regions of stability in Specimens 1 and 4 while Specimens 2 and 3 had notably smaller regions of stability (Figure 10). Results of the V/V model analysis showed much larger regions of stability across all specimens (Figure 11). Lastly, results of the F/E analysis using CT-based guides showed large regions of stability for all specimens (Figure 12). In these plots, blank areas represent parameter sets that do not come to rest in contact with the bone. The five circular data points in the F/E plots overlay the mean results of the corresponding guide technique from the cadaver lab.

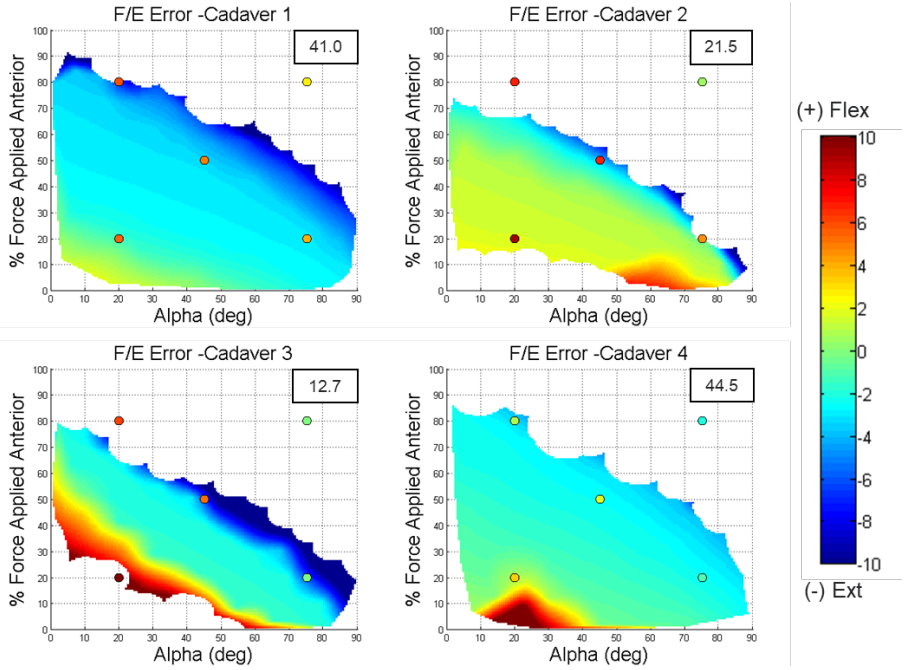

Figure 10: Flexion/extension error in degrees shown for the computational model of each bone using the XR-based guide across the range of techniques represented by the design space. Green represents 0 error compared to the surgical plan. The Guide Stability Score for each guide is inset in the top right.

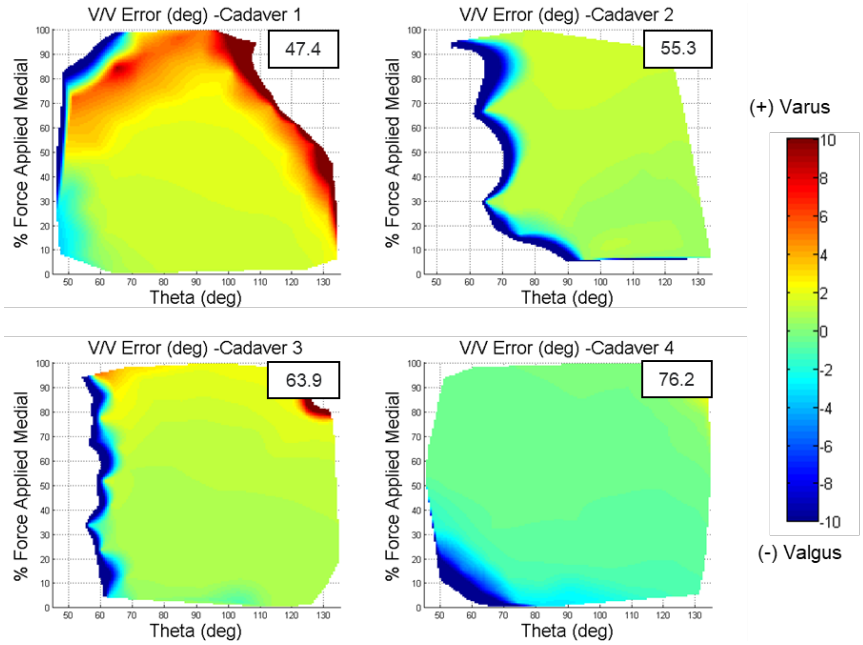

Figure 11: Varus/valgus error in degrees shown for each cadaver across the range of techniques represented by the design space. The Guide Stability Score for each guide is inset in the top right.

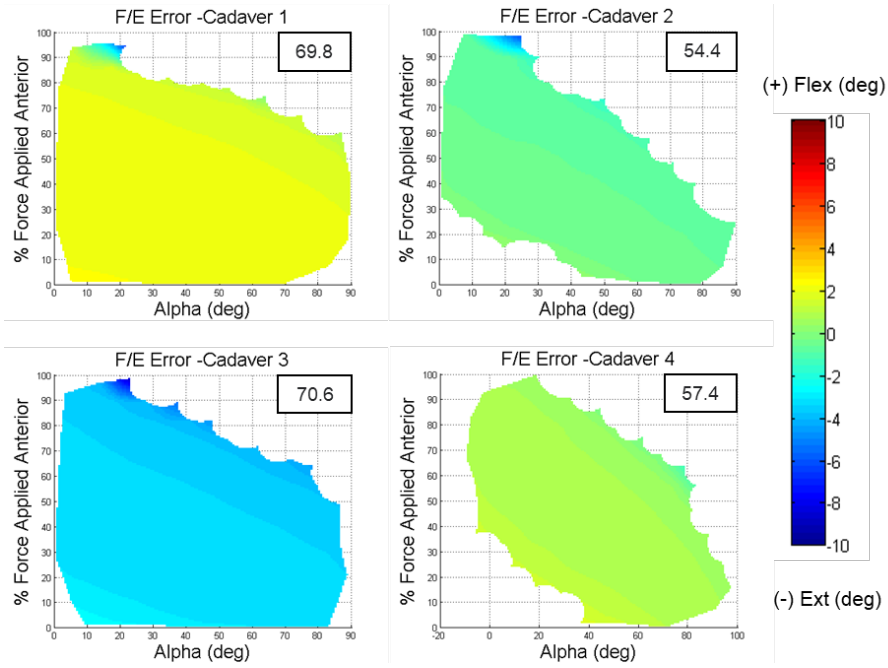

Figure 12: Flexion/extension error in degrees shown for CT-based guides which perfectly conform to the bone across the range of techniques represented by the design space. The Guide Stability Score for each guide is inset in the top right.

From the extracted Guide Stability Scores in the Flexion/Extension analysis, a linear regression was performed between the variance seen in the lab and the stability score predicted by the model across both the XR and CT models with a resulting r-squared value of 0.84.

Table 4: Cadaver lab flexion/extension standard deviation for XR-based guides compared to computational model guide stability score for XR-based guides and comparison of means between cadaver lab and model. Means and standard deviation from the lab are across all users and techniques.

	Lab Standard Deviation	***Guide Stability Score***	***Lab Mean***	***Model Mean***	***Cadaver Lab Flexion Bias***
Cadaver 1	1.30	41.0	4.38	-3.91	**8.29**
Cadaver 2	3.39	21.5	5.53	-0.91	**6.44**
Cadaver 3	5.18	12.7	4.23	-2.11	**6.34**
Cadaver 4	2.09	44.5	0.57	-1.81	**2.38**
All	-	-	3.68	-2.19	**5.86**

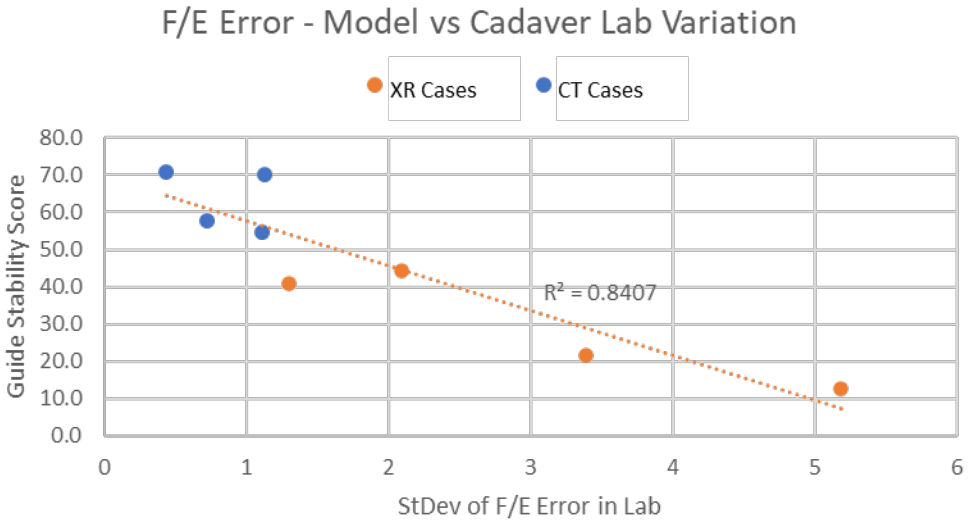

Figure 13: Correlation between standard deviation seen across all techniques in the lab and Guide Stability Score from the computational model.

Discussion and Conclusions

The results of the cadaver lab revealed that some specimens exhibited notably low variance in Flexion/Extension position (σ^2 = 1.3 deg) regardless of the operator or technique used to place the XR-based guide on the bone, while others varied by several degrees of flexion/extension error across techniques and operators (σ^2 = 5.2 deg), and even between runs of the same operator and technique.

A similar result was found in the computational model. The same specimen that had high consistency in the lab showed a stable response in Flexion/Extension error across a wide range of the guide positioning techniques represented by the design space, resulting in a high Guide Stability Score (GSS) of 41.0. The worst performing specimen from the lab which showed more variation between users and techniques displayed an unstable response in the model. For these guides, only a very small region of parameters for angle and distribution resulted in stable guide placement (GSS = 12.7).

The CT-based guide analysis in the computational model served as a control group for this study. Given the exact conformity between guide surface and bone, it was expected that these guides would score very high, which was seen in the results, averaging a stability score of 63.1 compared to the 29.9 average stability score seen in the XR-based guides.

The secondary analysis performed using the computational model for varus/valgus stability showed that the guides are all very stable in this axis, with low variance in the cadaver lab (σ^2 = 0.76, 0.36, 0.61, and 0.24 deg) and high model stability (GSS = 47.4, 48.3, 63.8, 74.3). This result was expected due to the design of the guides, where two

separate surfaces contact both medial and lateral distal condyles, providing a stable surface in this dimension.

One of the interesting differences between XR-based and CT-based guides was that the relative stability of the specimens did not match between these two guide designs. The worst performing cadaver for XR-based guides was the best performing CT-based guide. The most likely reason for this discrepancy is segmentation accuracy. The XR-based segmentations were compared to the CT-based segmentations to identify regions where major differences could result in guide instability. Cadaver 3 showed a particularly large undersegmentation on the medial and lateral edges of the anterior ridge. The lateral edge corresponds with a major contact area identified by the analysis which could account for the lack of stability in this guide. This identified region along with other contact points between guide and bone could be used to improve the XR-based segmentation in a way that targets and improves PSI guide stability.

In comparing the cadaver lab to the computational model, one deficiency of the model is clear in comparing the means of the two data sets, with the cadaver lab measuring an average of 5.9 degrees more flexion than the model predicted across all guides and techniques (Table 4). There are a few potential sources of this bias between the cadaver lab and model data. The registration process for the CAS acquired data can create bias in the lab data from model, particularly in acquisition of the hip center. Differences in the segmentation process for the XR-based guides compared to the CT-based guides could also create bias in the data between the two pre-operative planned resections, due to either the distal femur landmarks and/or the segmented hip center.

Even with the bias present in the data between the lab and model, similar trends between guide placement techniques were seen in both analyses. As expected in the cadaver lab, the anterior extension method for guide placement resulted in the most extended final position and the distal flexion method resulted in the most flexed final position, with the remaining methods falling in between those two limits. This trend was mirrored in the computational model (Figure 10), where the results showed that the anterior extension corner of the plot predicts the most extension and the distal flexion corner of the plot predicts the most flexion.

This method of analysis created a Guide Stability Score that correlated well with variance observed experimentally in the cadaver lab setting, suggesting this method offers valuable insight into how robust a guide fit will be for a given patient. Based on the limited available data from this study, a Guide Stability Score of greater than 30 correlates well with a robust bone/guide pair. For the samples of this analysis, high scores correlated with consistent guide placement across a wide variety of users and techniques. The ceiling for the Guide Stability Score seems to be around 70, corresponding to the best result from a perfect fitting CT-based guide, Cadaver 3.

The Guide Stability Score does vary significantly from patient to patient, so using this tool to evaluate how robust a specific guide may be in a surgical setting is a use case which could have immediate impact. Using the tool to compare different prototype guide designs would need to be performed across a large sample of patients to establish which design would perform the best across a wide population of cadavers. The specific geometries that contribute to a guide and cadaver pair having a high or low Guide

Stability Score could not be precisely identified from this study after examination of the contact area maps for both XR-based and CT-based guides, though there is evidence to suggest segmentation error in the anterior ridge region contribute to these differences. While the CT-based guides had higher contact areas (mean = 135 mm^2) than the XR-based guides (mean = 60 mm^2) due to conformity between the bone and guide, there was no strong correlation found between contact area and Guide Stability Score. Identifying which regions of the bone most contribute to a stable guide configuration will continue to be an area for further study.

After examining the results of the computational model, a region of parameter values was identified where every bone/guide pair showed a stable response. This region was identified during the flexion/extension analysis as a 40% anterior distribution of force and angle of 30 deg. This finding could be used to reevaluate the instructions in a PSI surgical technique to give the surgical user the highest likelihood of success in finding a stable configuration for the PSI guide.

One limitation of this tool is that two different bone geometries are needed for the tool to function properly. For this study, both CT and x-ray imaging was available. For typical patients, that is not a viable option. As illustrated from the CT-based guides paired with CT bones, simply relying on one imaging modality to evaluate a guide and the identical bone from which it was created results in an artificially high Guide Stability Score. When identical geometries were used for the analysis, even the worst performing guide scored a 54.4 for Guide Stability Score. Ideally, an optical scan of the bone would be available as the true bone geometry could then be used to evaluate both CT-based and

XR-based guide for further development of this model. This could alternatively be achieved through different segmentation methods of the same imaging data or potentially through statistical shape modeling-based perturbation in the bone geometry to ensure an imperfect fit.

Refinement of the current model could be pursued through adjustment of the contact parameters between guide and bone. Using separate pressure-overclosure models for the cartilage contacting surfaces of the guide versus the bone contacting surfaces of the guide may improve the ability of the model represent cadaver lab results. Improving or further separating the simplified loading used in this analysis may also improve results beyond what was achieved in this study.

This model successfully represented the variance seen experimentally. The accuracy of the guide showed unexpected bias, but there was still a strong correlation between the guide stability score and the variance seen in the lab, suggesting the model provides a novel tool for the evaluation of PSI guide design stability. This study exposed the large differences in stability that can occur between patients, even with the same guide design. Ideally, a prototype guide design would be analyzed using this model across a wide range of patients and then the highest average stability score across that patient population could be used to cull guide designs down to a select few for surgical evaluation.

Bibliography

Broeck JV den, W.-S. R. (2015). Preoperative analysis of the stability of fit of a patient-specific surgical guide. *Comput Method Biomec,* 38-47. doi:10.1080/10255842.2013.774383

Darby E., S. C. (2020). EXPERIMENTAL ANALYSIS OF THE DOCKING RIGIDITY OF PATIENT-SPECIFIC GUIDES. *Orthopaedic Proceedings, 102-B, No. SUPP_2,* pp. 30-30. Toronto.

Halloran JP, E. S. (2005, Oct). Comparison of deformable and elastic foundation finite element simulations for predicting knee replacement mechanics. *J Biomech Eng, 127*(5), 813-8. doi:10.1115/1.1992522

Kim, Y. P. (2014). The relationship between the survival of total knee arthroplasty and postoperative coronal, sagittal and rotational alignment of knee prosthesis. *International Orthopaedics (SICOT), 38,* 379–385. doi:https://doi.org/10.1007/s00264-013-2097-9

Kunz M, R. J. (2010). Computer-Assisted Hip Resurfacing Using Individualized Drill Templates. *J Arthroplasty, 25*(4), 600-606. doi:10.1016/j.arth.2009.03.023

Mattei L, P. P. (2016). Patient specific instrumentation in total knee arthroplasty: a state of the art. *Ann Transl Medicine, 4*(7), 126-126. doi:10.21037/atm.2016.03.33

Mattheijer J, H. J. (2013). Shaping Patient Specific Surgical Guides for Arthroplasty to Obtain High Docking Robustness. *J Mech Design, 135*(7), 071001. doi:10.1115/1.4024231

Mattheijer J, H. J. (2015). Docking Robustness of Patient Specific Surgical Guides for Joint Replacement Surgery. *J Mech Design, 137*(6), 062301. doi:10.1115/1.4029665

Mueller S, M. E. (2016). Intraoperative Verification of Patient Specific Instrument Orientation using 2D Imaging with Embedded References. *CURAC 2016 Proceedings*, (pp. 71-76). Bern.

Appendix A

Table 5: Raw recorded data from the Knee3 CAS System used for the cadaver lab portion of this study.

Cadaver Number	Side	Bone	User	Guide Imaging	Method	Run	F/E (deg)	V/V (deg)	Med Resect (mm)	Lat Resect (mm)
1	L	Femur	1	XR	Anterior Extension	1	1.5	0	10	6
1	L	Femur	1	XR	Freestyle	1	4	0.5	10	6.5
1	L	Femur	1	XR	Distal Flexion	1	5.5	0.5	10.5	6.5
1	L	Femur	1	XR	Distal Extension	1	4	0	10.5	7
1	L	Femur	1	XR	Anterior Flexion	1	5	0	11	7.5
1	L	Femur	2	XR	Anterior Extension	1	2.5	0	10.5	7
1	L	Femur	3	XR	Freestyle	1	5	-0.5	11	8
1	L	Femur	3	XR	Distal Flexion	1	5.5	-0.5	11	8
1	L	Femur	3	XR	Distal Extension	1	4	0	10.5	7.5
1	L	Femur	3	XR	Anterior Flexion	1	6.5	0	11	7.5
1	L	Femur	2	XR	Freestyle	1	5	0	10.5	7.5
1	L	Femur	2	XR	Distal Flexion	1	5.5	-0.5	11	8
1	L	Femur	2	XR	Distal Extension	1	4	0	11	7.5
1	L	Femur	2	XR	Anterior Flexion	1	5.5	0.5	11	7.5
1	L	Femur	3	XR	Anterior Extension	1	3.5	0	10.5	7.5
1	L	Femur	1	XR	Freestyle	1	3	-2	10.5	6
1	L	Femur	1	XR	Freestyle	2	3.5	-2	10	5.5
1	L	Femur	1	XR	Freestyle	3	4	-2	10	5.5
1	L	Femur	2	XR	Freestyle	1	3.5	-2.5	10.5	7
1	L	Femur	2	XR	Freestyle	2	5	-2.5	10.5	6.5
1	L	Femur	2	XR	Freestyle	3	5.5	-2.5	10.5	6
1	L	Femur	3	XR	Freestyle	1	3.5	-3	10.5	6.5
1	L	Femur	3	XR	Freestyle	2	4.5	-2	11	7

1	L	Femur	3	XR	Freestyle	3	4.5	-2	11	6
2	L	Femur	1	XR	Freestyle	1	6	-3	9	5
2	L	Femur	1	XR	Distal Flexion	1	10.5	-2.5	9.5	6
2	L	Femur	1	XR	Distal Extension	1	5	-3	9	5.5
2	L	Femur	1	XR	Anterior Flexion	1	6	-3	8	8
2	L	Femur	3	XR	Freestyle	1	4.5	-3	9.5	5.5
2	L	Femur	3	XR	Distal Flexion	1	5.5	-3	9.5	5.5
2	L	Femur	3	XR	Distal Extension	1	2.5	-3	9.5	6
2	L	Femur	3	XR	Anterior Flexion	1	7.5	-3	9.5	6
2	L	Femur	2	XR	Anterior Extension	1	-1	-2.5	9.5	5
2	L	Femur	2	XR	Freestyle	1	6	-2.5	9	5
2	L	Femur	2	XR	Distal Flexion	1	11.5	-2	10	6.5
2	L	Femur	2	XR	Distal Extension	1	6	-3	9.5	5.5
2	L	Femur	2	XR	Anterior Flexion	1	7	-2.5	9.5	5.5
2	L	Femur	3	XR	Anterior Extension	1	1	-3	9.5	5.5
2	L	Femur	1	XR	Anterior Extension	1	1.5	-3	9	5.5
2	L	Femur	1	XR	Freestyle	1	6	-2	10	6.5
2	L	Femur	1	XR	Freestyle	2	6.5	-2.5	10	7
2	L	Femur	1	XR	Freestyle	3	6.5	-2	11	7.5
2	L	Femur	2	XR	Freestyle	1	7.5	-2	10.5	7.5
2	L	Femur	2	XR	Freestyle	2	8.5	-2	9.5	6.5
2	L	Femur	2	XR	Freestyle	3	8.5	-2	10	7.5
2	L	Femur	3	XR	Freestyle	1	7	-2	10	7.5
2	L	Femur	3	XR	Freestyle	2	5.5	-3	10.5	7.5
2	L	Femur	3	XR	Freestyle	3	7.5	-2	10.5	7.5
3	L	Femur	1	XR	Freestyle	1	3	1	9	9
3	L	Femur	1	XR	Distal Flexion	1	10.5	2.5	9	8
3	L	Femur	1	XR	Distal Extension	1	-0.5	2	9	8.5
3	L	Femur	1	XR	Anterior Flexion	1	10	2	8.5	7.5

3	L	Femur	3	XR	Freestyle	1	2.5	1	9.5	9.5
3	L	Femur	3	XR	Distal Flexion	1	12	1	9.5	9.5
3	L	Femur	3	XR	Distal Extension	1	0	1.5	10	9.5
3	L	Femur	3	XR	Anterior Flexion	1	8.5	1	9	9
3	L	Femur	2	XR	Anterior Extension	1	-3	2	9.5	8.5
3	L	Femur	2	XR	Freestyle	1	5	1	9	9
3	L	Femur	2	XR	Distal Flexion	1	9	2	9.5	8
3	L	Femur	2	XR	Distal Extension	1	-0.5	2.5	9.5	8.5
3	L	Femur	2	XR	Anterior Flexion	1	0	1	9	9
3	L	Femur	3	XR	Anterior Extension	1	-1.5	1.5	9.5	9
3	L	Femur	1	XR	Anterior Extension	1	3.5	1.5	8	8
3	L	Femur	1	XR	Freestyle	1	6	1	9.5	7
3	L	Femur	1	XR	Freestyle	2	1	0.5	9	7.5
3	L	Femur	1	XR	Freestyle	3	1	0.5	10	8
3	L	Femur	2	XR	Freestyle	1	10	1	11	9
3	L	Femur	2	XR	Freestyle	2	12.5	0.5	11	9
3	L	Femur	2	XR	Freestyle	3	12	1	10	8
3	L	Femur	3	XR	Freestyle	1	1.5	1	10	8
3	L	Femur	3	XR	Freestyle	2	1.5	0	10	8.5
3	L	Femur	3	XR	Freestyle	3	6	1	10.5	8
4	L	Femur	2	XR	Anterior Extension	1	-3.5	-3	8.5	7.5
4	L	Femur	1	XR	Anterior Extension	1	-2	-2	8	6
4	L	Femur	3	XR	Anterior Extension	1	-0.5	-2	9.5	8
4	L	Femur	1	XR	Freestyle	1	-0.5	-1.5	9.5	7.5
4	L	Femur	1	XR	Distal Flexion	1	2.5	-2	9	8
4	L	Femur	1	XR	Distal Extension	1	-1.5	-2	9	7.5
4	L	Femur	1	XR	Anterior Flexion	1	1	-1.5	8.5	7
4	L	Femur	3	XR	Freestyle	1	-1	-2	9.5	7

4	L	Femur	3	XR	Distal Flexion	1	4.5	-2	9	7.5
4	L	Femur	3	XR	Distal Extension	1	-1	-2	9.5	7.5
4	L	Femur	3	XR	Anterior Flexion	1	1.5	-1.5	9.5	7.5
4	L	Femur	2	XR	Freestyle	1	-0.5	-2.5	9.5	8
4	L	Femur	2	XR	Distal Flexion	1	2.5	-2	9.5	8
4	L	Femur	2	XR	Distal Extension	1	-0.5	-2	9.5	7.5
4	L	Femur	2	XR	Anterior Flexion	1	0	-2.5	9.5	8.5
4	L	Femur	1	XR	Freestyle	1	2	-2	8.5	6.5
4	L	Femur	1	XR	Freestyle	2	2.5	-2	9.5	7
4	L	Femur	1	XR	Freestyle	3	2.5	-2	9.5	7
4	L	Femur	2	XR	Freestyle	1	3.5	-2	9.5	7.5
4	L	Femur	2	XR	Freestyle	2	2.5	-2.5	9	7.5
4	L	Femur	2	XR	Freestyle	3	3	-2	9.5	7.5
4	L	Femur	3	XR	Freestyle	1	3	-2	9.5	7
4	L	Femur	3	XR	Freestyle	2	2.5	-2	9.5	7.5
4	L	Femur	3	XR	Freestyle	3	2.5	-2.5	9.5	7.5

Cadaver Number	Side	Bone	User	Guide Imaging	Method	Run	F/E (deg)	V/V (deg)	Med Resect (mm)	Lat Resect (mm)
1	L	Femur	1	CT	Freestyle	1	5	-2.5	10.5	6.5
1	L	Femur	1	CT	Freestyle	2	4.5	-2.5	10.5	6.5
1	L	Femur	1	CT	Freestyle	3	4.5	-2	10.5	6.5
1	L	Femur	2	CT	Freestyle	1	6	-2.5	10.5	6.5
1	L	Femur	2	CT	Freestyle	2	7	-2.5	11	7
1	L	Femur	2	CT	Freestyle	3	7.5	-2	11.5	7
1	L	Femur	3	CT	Freestyle	1	5	-2	11	6.5
1	L	Femur	3	CT	Freestyle	2	5	-2	10.5	6.5
1	L	Femur	3	CT	Freestyle	3	4.5	-2	10.5	6
2	L	Femur	1	CT	Freestyle	1	5	-2	10	6.5
2	L	Femur	1	CT	Freestyle	2	7	-2	10	7
2	L	Femur	1	CT	Freestyle	3	7	-2.5	10.5	7.5
2	L	Femur	2	CT	Freestyle	1	8.5	-3	10	8.5

2	L	Femur	2	CT	Freestyle	2	8.5	-3	10.5	8.5
2	L	Femur	2	CT	Freestyle	3	8	-3.5	10	9
2	L	Femur	3	CT	Freestyle	1	7	-3	10	7.5
2	L	Femur	3	CT	Freestyle	2	8	-3	10	8
2	L	Femur	3	CT	Freestyle	3	6.5	-2	11	7.5
3	L	Femur	1	CT	Freestyle	1	1.5	-1	9.5	8.5
3	L	Femur	1	CT	Freestyle	2	1.5	0	10	9
3	L	Femur	1	CT	Freestyle	3	1.5	-0.5	10.5	9
3	L	Femur	2	CT	Freestyle	1	2	-0.5	10	9
3	L	Femur	2	CT	Freestyle	2	2.5	0	10	9
3	L	Femur	2	CT	Freestyle	3	2.5	-0.5	10	9
3	L	Femur	3	CT	Freestyle	1	1.5	-0.5	10	9
3	L	Femur	3	CT	Freestyle	2	1.5	-0.5	10	9
3	L	Femur	3	CT	Freestyle	3	1.5	-1	10	9
4	L	Femur	1	CT	Freestyle	1	4	-1.5	10	7.5
4	L	Femur	1	CT	Freestyle	2	4.5	-1.5	10	7
4	L	Femur	1	CT	Freestyle	3	4	-1.5	10	7.5
4	L	Femur	2	CT	Freestyle	1	5.5	-1	10	7.5
4	L	Femur	2	CT	Freestyle	2	5	-1	10.5	7
4	L	Femur	2	CT	Freestyle	3	5	-1	10	7.5
4	L	Femur	3	CT	Freestyle	1	4.5	-1	10.5	7.5
4	L	Femur	3	CT	Freestyle	2	4.5	-1.5	10.5	8
4	L	Femur	3	CT	Freestyle	3	3	-2.5	9.5	8

Appendix B

All sensitivity analyses plotted the equilibrium position data of the guide for Cadaver 1 as a function of the variable being tested. Position plots show X, Y, Z data in mm and rotation plots show flexion/extension, varus/valgus, (and internal/external) data in degrees.

Table 6: Results of sensitivity analyses for each of Mesh Density, Friction, Pressure Overclosure, and Initial Perturbation

Variable	*Value*	*F/E Rot*	*V/V Rot*	*I/E Rot*	*M/L*	*A/P*	*I/S*
Mesh Edge Length	0.50	1.16	2.60	0.17	0.99	1.16	-1.16
	0.75	1.37	2.46	0.01	1.02	1.08	-0.94
	1.20	1.37	2.46	0.01	1.02	1.08	-0.94
Friction	0.002	-4.01	0.76	0.24	0.87	5.11	5.40
	0.01	-3.90	0.61	0.26	0.89	5.11	5.30
	0.05	-3.96	0.46	0.73	1.04	4.72	5.16
	0.1	-4.08	0.52	0.61	1.20	4.68	5.18
	0.2	-2.02	0.36	0.82	2.16	4.98	4.08
	0.3	-1.12	1.02	-1.02	3.00	6.25	3.73
Pressure Overclosure	0.1	-2.62	2.34	-3.92	-3.48	6.28	6.85
	0.25	-2.79	2.12	-3.05	-2.40	6.12	6.66
	1	-2.75	1.55	-1.71	-0.72	6.27	6.36
	4	-2.89	1.46	-1.41	-0.29	6.18	6.28
	10	-2.93	1.61	-1.86	-0.74	6.02	6.27
Initial Position	0,0,0	-2.93	1.61	-1.86	-0.74	6.02	6.27
	1,1,1	-2.93	1.62	-1.88	-0.78	6.03	6.27
	-1,1,1	-2.92	1.62	-1.87	-0.77	6.03	6.27
	1,-1,1	-2.95	1.54	-1.64	-0.48	6.06	6.26
	1,1,-1	-2.95	1.44	-1.41	-0.20	6.11	6.26
	-1,-1,-1	-2.95	1.43	-1.36	-0.16	6.11	6.26

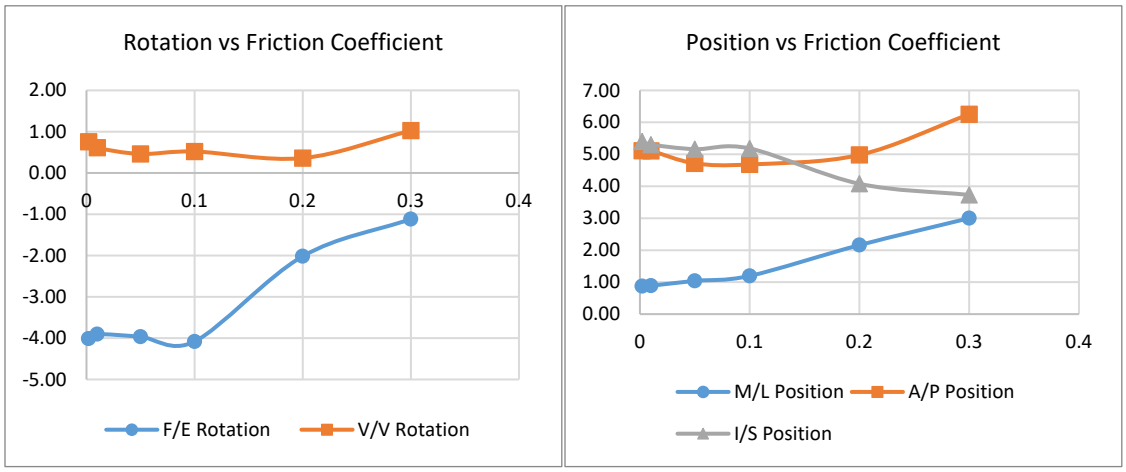

Figure 14: Plots showing the response of the guide position at equilibrium as a function of friction coefficient

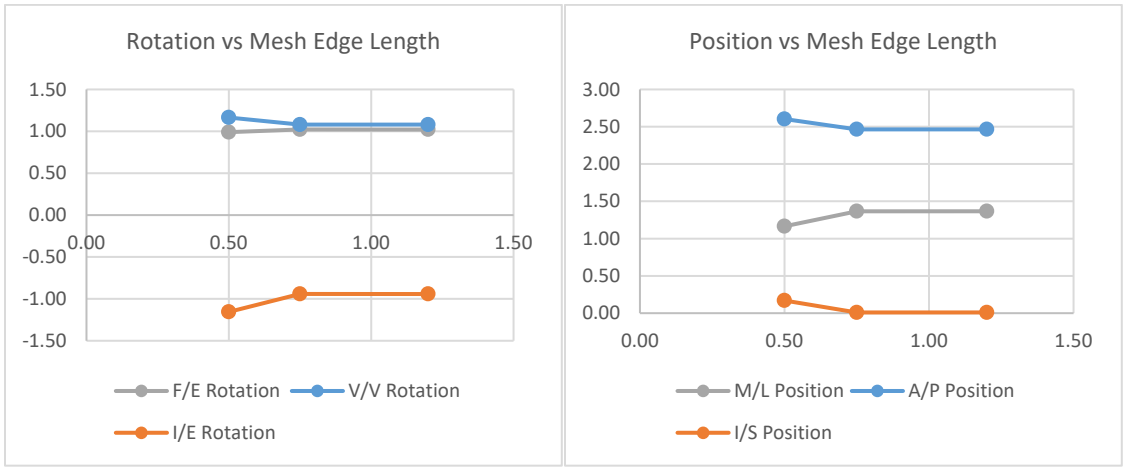

Figure 15: Plots showing the response of the guide position at equilibrium as a function of mesh edge length

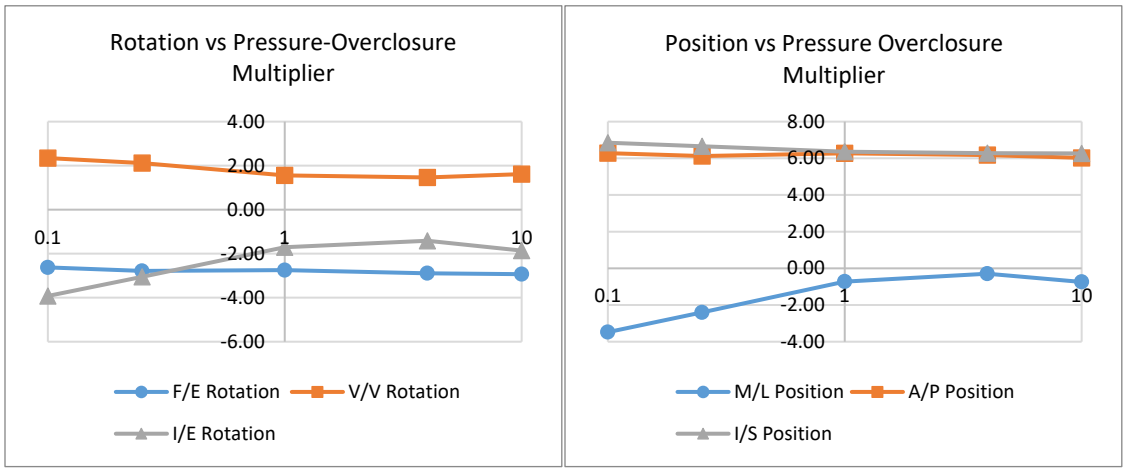

Figure 16: Plots showing the response of the guide position at equilibrium as a function of pressure-overclosure multiplier

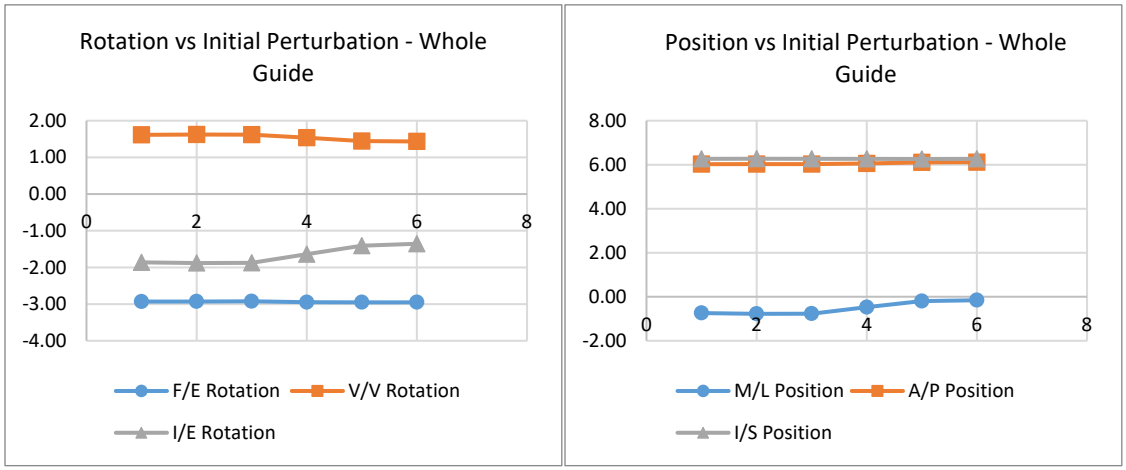

Figure 17: Plots showing the response of the guide position at equilibrium as a function of initial perturbation, see table above for key of perturbations.